Supplementary Materials and Methods

Barrier function assays

At E17.5, the embryos were rinsed in phosphate-buffered saline (PBS) and immersed in acidic X-gal mix (100 mM phosphate buffer at pH4.3, 3 mM $K_3Fe(CN)_6$, 3 mM $K_4Fe(CN)_6$, 2 mM $MgCl_2$, 1 mg/mL X-gal), then incubated for 8 hours at 37℃ in the dark.

Quantitative real-time PCR

Total RNAs from tissues were extracted using Trizol (Gibco). cDNA was generated using the Invitrogen SS II RT kit. Expression of genes indicated in the text was measured by real-time qRT-PCR, and normalized to GAPDH expression levels.

Plasmid Construction

Site-directed PCR mutagenesis was used to introduce the missense changes S61A, S109A, S127A, T328A and S347A into the YAP sequence. The cDNAs for YAP and its serine to alanine (SA) mutant form were cloned into pET-15b (Novagen) to generate recombinant hexahistidine (His6)-tagged YAP and SA proteins, respectively.

In-vitro Kinase Assay

Immunoprecipitated HA-LATS1/2-WT or -KD were incubated for 30 minutes at 30℃ with purified His-YAP-WT or His-YAP-SA in kinase buffer (25 mM HEPES pH 7.4, 50 mM NaCl, 5 mM $MgCl_2$, 5 mM $MnCl_2$, 5 mM β-glycerophosphate and 1 mM dithiothreitol) supplemented with 10 μM adenosine 5'triphosphate (ATP) and 2 μCi [γ-^{32}P]ATP. Reaction mixtures were analyzed by SDS-PAGE and autoradiography to detect ^{32}P-labeled YAP.

Supplementary Table and Figure Legends

Supplementary Table1. Genotypes of progeny from WW45 heterozygous intercrosses

Supplementary Figure S1. Defective vascularization of WW45$^{-/-}$ placenta at E17.5. Extra-embryonic vascular defects were confirmed by immunohistochemistry analysis with antibodies against PECAM-1 and laminin. Scale bar: 100 μm.

Supplementary Figure S2. Hyperplasia in WW45$^{-/-}$ epithelial tissues at E17.5. Histological analysis of hematoxylin & eosin (H&E)-stained sections of wild-type (a–d) or mutant (a'–d') epithelial tissues. (a, a') Large intestine. (b, b') Lung. (c, c') Retina. (d, d') Tongue. Note the dense and disorganized epithelia in mutant embryos. Scale bar: 100 μm.

Supplementary Figure S3. Dysmaturation of skin barrier function in mutant embryo at E17.5. Skin barrier function assay by X-gal staining. Blue-dye incorporation represents disruption to formation of the epidermal barrier in mutant embryos compared with their wild-type littermates.

Supplementary Figure S4. Hyperproliferation in WW45$^{-/-}$ epithelial tissues at E17.5. (A) Evaluation of cellular proliferation in wild-type or mutant colonic epithelium by co-immunohistochemistry analysis with anti-Ki67 and anti-β-catenin. Note the increased numbers of Ki67-positive cells, including those located in multiple cell layers, in the mutant epithelium compared with the control epithelium; in the control epithelium, Ki67-positive cells were present mainly in the restricted proliferation zone. Scale bar: 100 μm. **(B)** Quantitative analysis of the percentage of BrdU-positive cells per 1.0-mm^2 area of epithelium 2 hours after BrdU injection. Data represent triplicate independent experiments ±SD.

Supplementary Figure S5. Defective cell-cycle exit in WW45$^{-/-}$ keratinocytes. (A and B) BrdU-labeling index of keratinocytes cultured with or without transforming growth factor (TGF)-β (A) or LiCl (B). Note the failure to stop cycling in WW45-deficient keratinocytes in response to TGF-β or LiCl treatment.

Supplementary Figure S6. Requirement of WW45 for interaction between MST1/2

and LATS1/2 in primary keratinocytes. Physical associations between MST1, LATS1/2, WW45 and YAP under differentiation conditions. $WW45^{-/-}$ primary keratinocytes were co-transfected with the plasmids indicated at the top of each panel. After 24 hours of transfection, cells were maintained in Ca^{2+}-containing medium for a further 24 hours before harvesting for immunoprecipitation with anti-hemagglutinin (HA). The resulting precipitates were subjected to Western-blot analysis with the indicated antibodies. Note that complex formation was only detected in the presence of WW45.

Supplementary Figure S7. Phosphorylation of YAP serine 127 by LATS1/2 in the MST1 pathway is induced by differentiation signals in primary keratinocytes. (A) Partial alignment of the conserved regions of YAP with the *Drosophila* Yki protein. The consensus motif of the site phosphorylated by LATS1/2 is underlined. Asterisk indicates the YAP serine 127 residue, which is the phosphorylation site for LATS1/2. **(B)** Identification of the phosphorylation site of YAP. WW45-deficient primary keratinocytes were co-transfected with the indicated plasmids and probed with the indicated antibodies. **(C)** *In-vitro* kinase assays using immunoprecipitated HA-tagged LATS1/2 WT or KD and purified His-YAP-WT or His-YAP-SA were performed, and the signals are shown by autoradiography analysis (top two panels). The input kinase and substrate for Western-blot analysis using anti-LATS1/2 and anti-YAP are also shown (bottom two gels). **(D)** Western-blot analysis with anti-YAP or an antibody specific for the serine-127-phosphorylated YAP (p-YAP) in wild-type and mutant primary keratinocytes cultured with or without Ca^{2+} for 24 hours. Differentiation of keratinocytes and the presence of WW45 were assessed by Western-blot analysis using anti-filaggrin and anti-WW45.

Supplementary Figure S8. Verification of the MST1 antibody. (A) Western-blot analysis was performed with lysates of HeLa cells stably transfected with a vector encoding MST1 siRNA or GFP siRNA as a control. α-tubulin was used as a loading control. **(B)** Control- and MST1-siRNA-expressing HeLa cells were stained with DAPI and with MST1 antibody.

Supplementary Figure S9. Nuclear localization of YAP in proliferative progenitor compartment of the small intestine. The serial sections of the wild-type embryos were stained with anti-YAP and anti Ki67. Note the nuclear-localized YAP in the Ki67-positive cycling cells of the crypt compartment of the small intestine. Scale bar: 100μm.

Supplementary Figure S10. Expansion of progenitor cells and loss of differentiated cells in WW45$^{-/-}$ epithelium. (A) Representative H&E and anti-K1 stained sections of epidermis from control and mutant embryos at the indicated developmental stages. Note the expansion of the K1-positive progenitor layers in the developing WW45$^{-/-}$ epidermis. **(B)** Representative H&E-stained sections of intestine (B) from control and mutant embryos at the indicated developmental stages. Note the increased cellularity with defective terminal differentiation in the developing WW45$^{-/-}$ embryos. Scale bar: 100 μm.

Supplementary Figure S11. Increased proliferation in WW45$^{-/-}$ epithelium onset of terminal differentiation. Comparison of the numbers of Ki67-positive cells (average number per 1.0-mm^2 area) in wild-type and mutant epithelia at the indicated developmental stages. Data represent triplicate independent experiments ±SD.

Supplementary Figure S12. Quantitative RT-PCR analysis. RNA isolated from wild-type and mutant epidermis was analyzed by quantitative RT-PCR. Data represent triplicate independent experiments ±SD.

Supplemental Table 1

Table1. Genotypes of progeny from WW45 heterozygous intercrosses

Age (dpc)	No. per genotype			
	+/+	+/-	-/-	Total
17.5	168	352	85	605
18.0	17	34	6	57
18.5	22	45	5	72
19.0	4	2	0	6
Neonates	350	601	3	954

Supplemental Figure S1

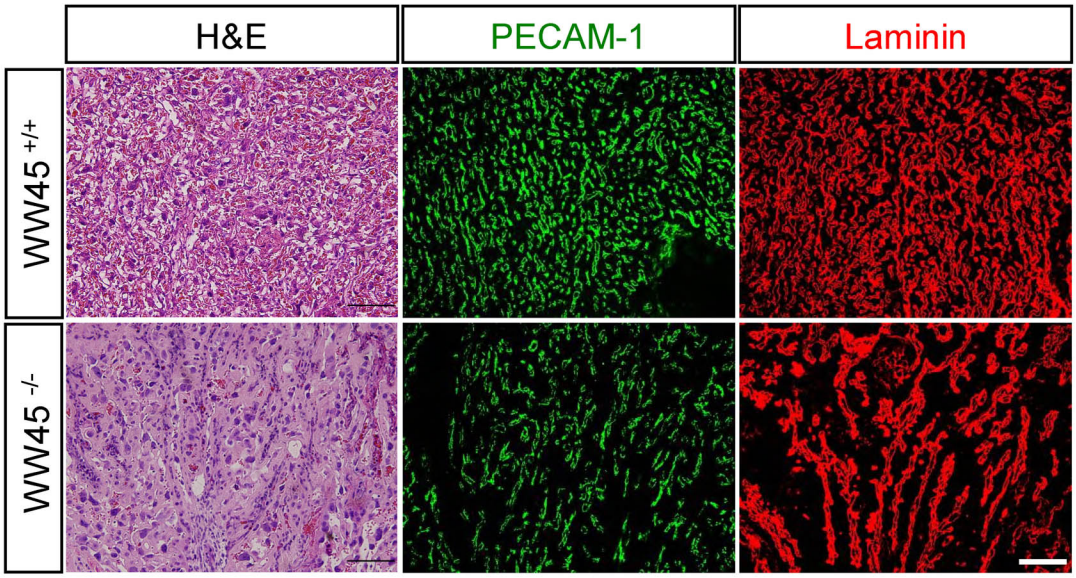

Supplemental Figure S2

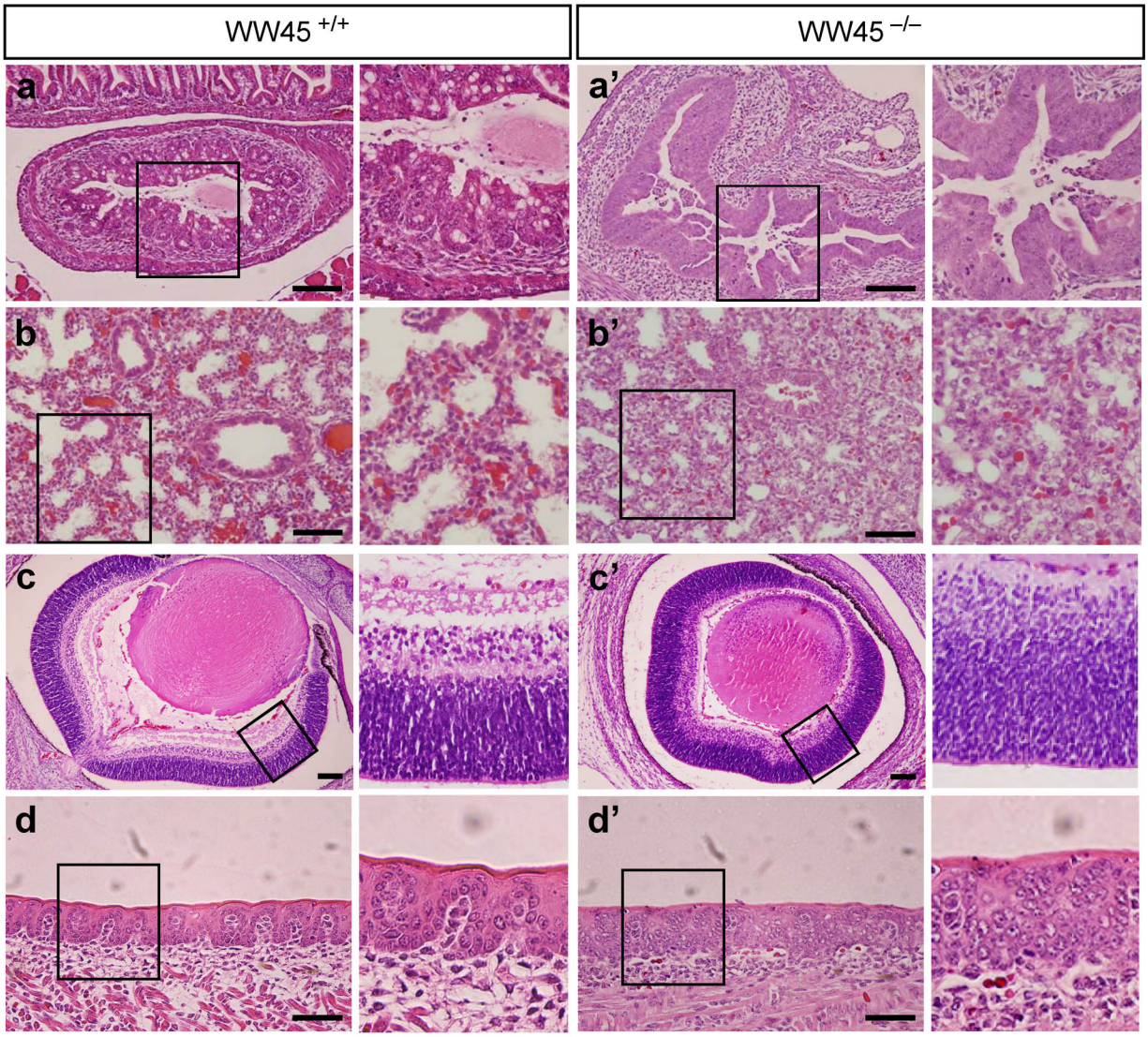

Supplemental Figure S3

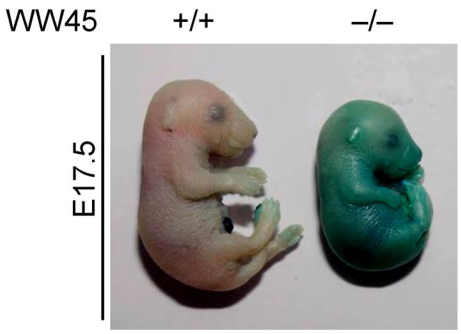

Supplemental Figure S4

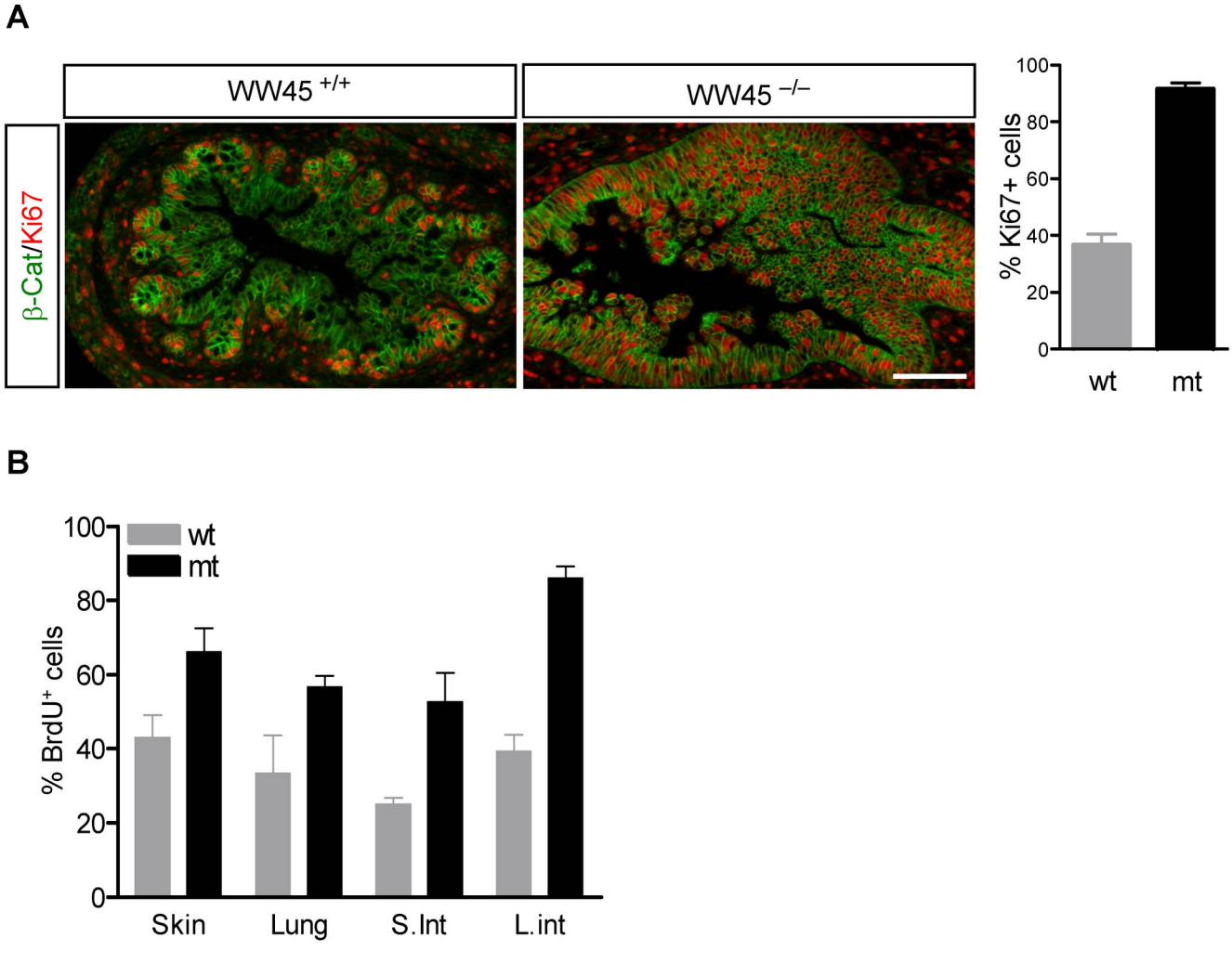

Supplemental Figure S5

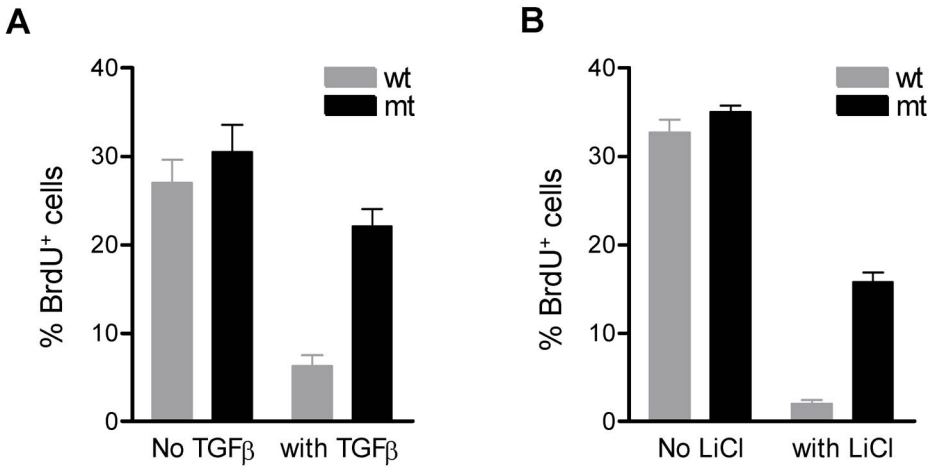

Supplemental Figure S6

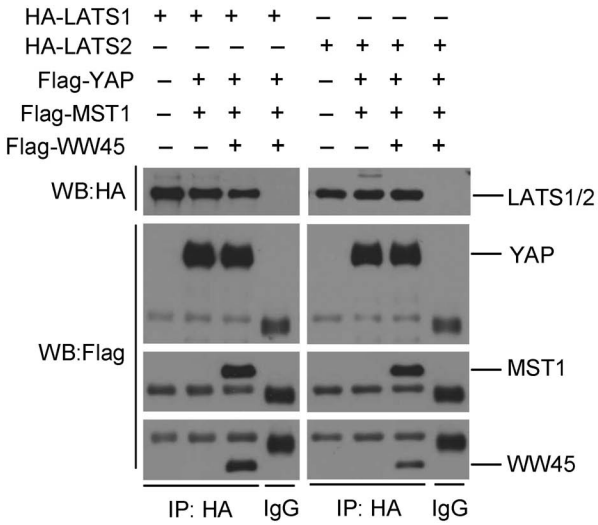

Supplemental Figure 7

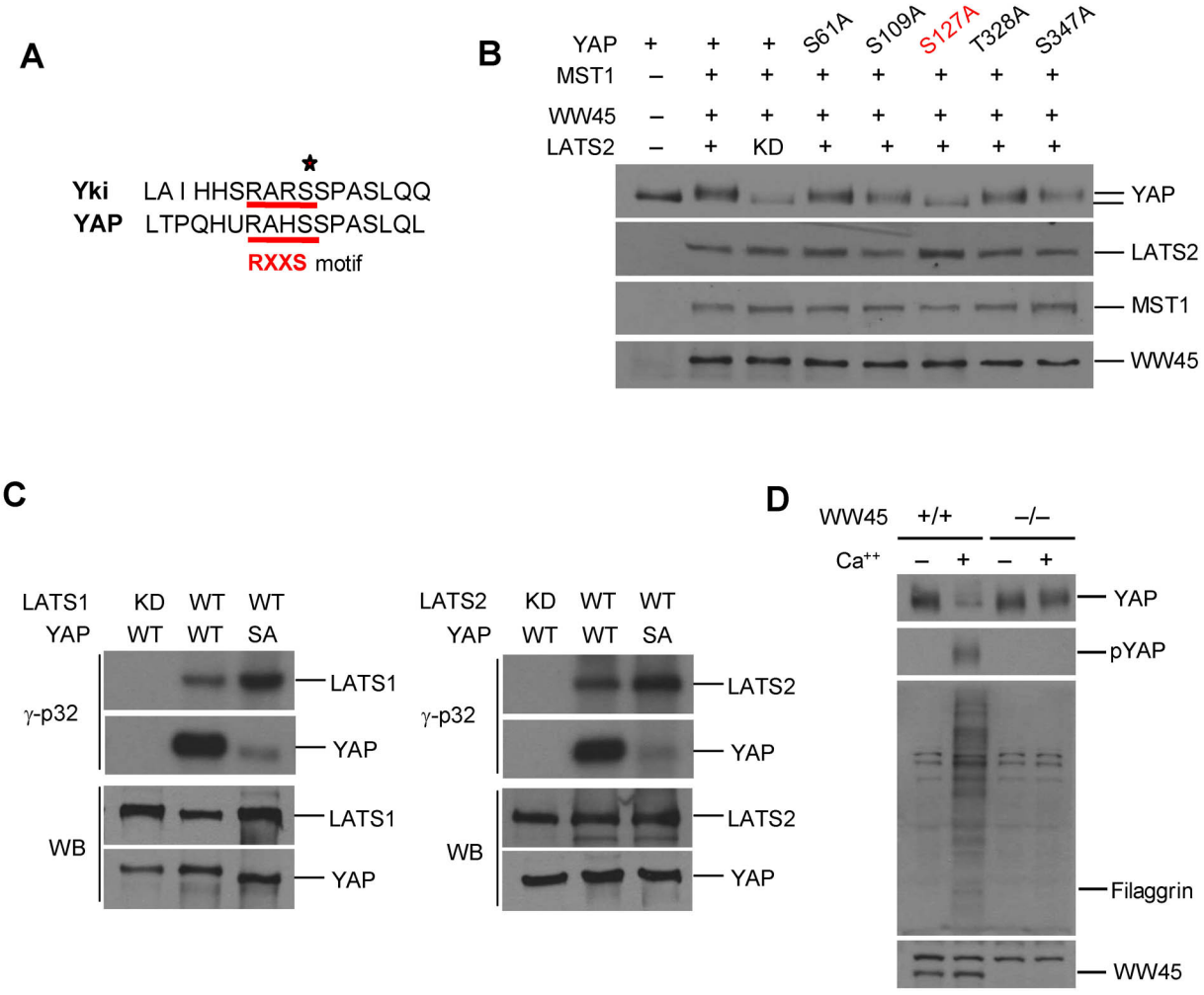

Supplemental Figure S8

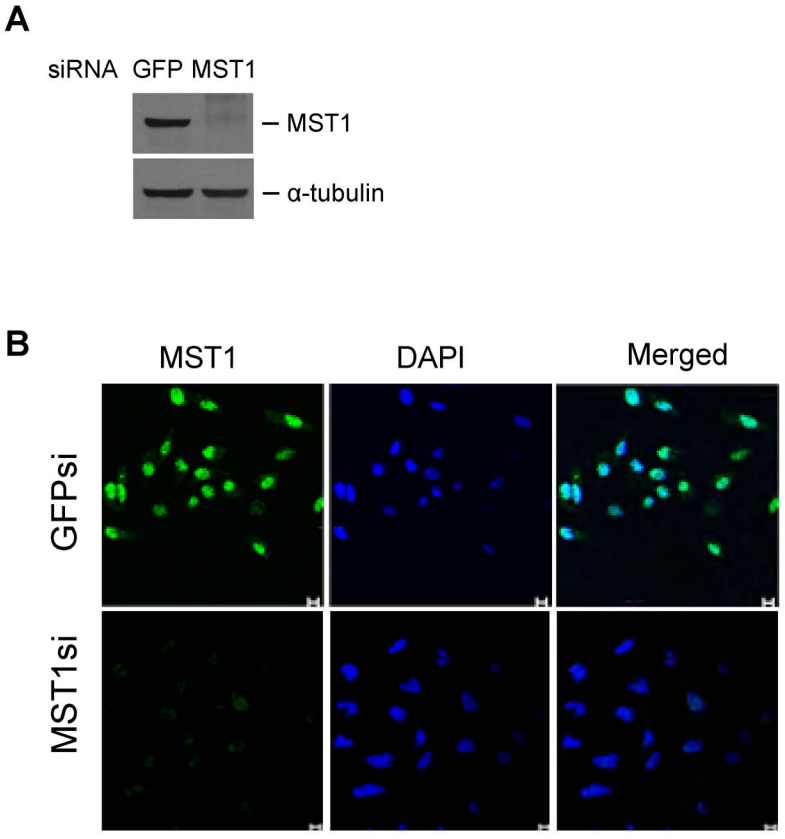

Supplemental Figure S9

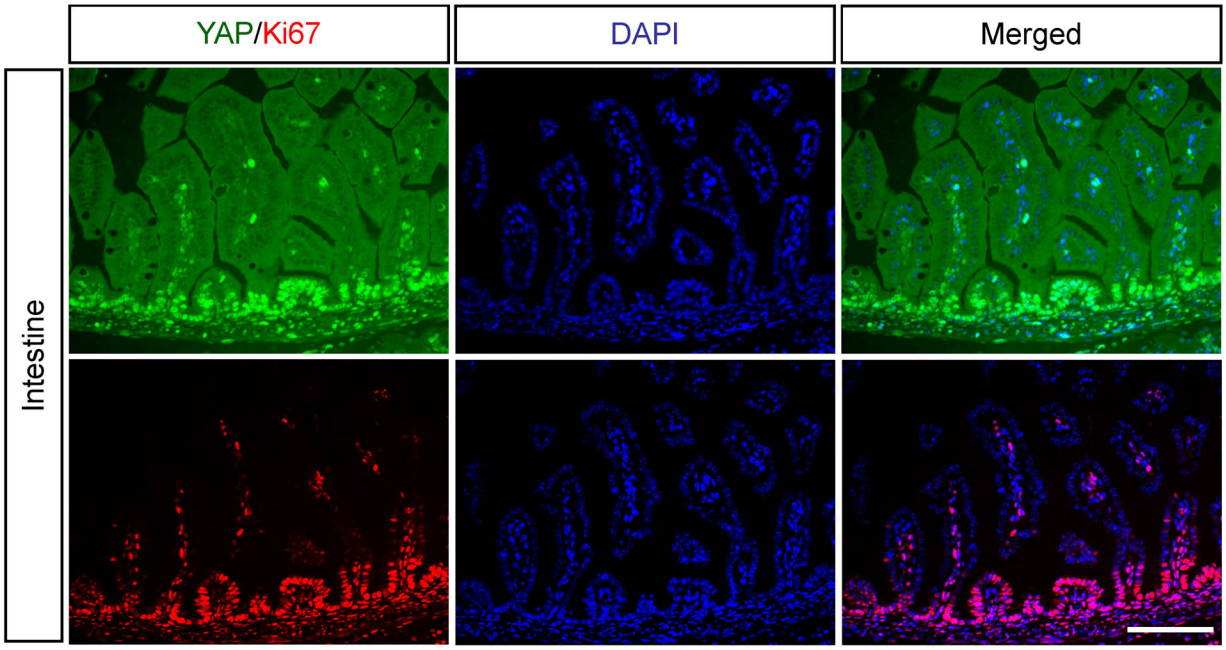

Supplemental Figure S10

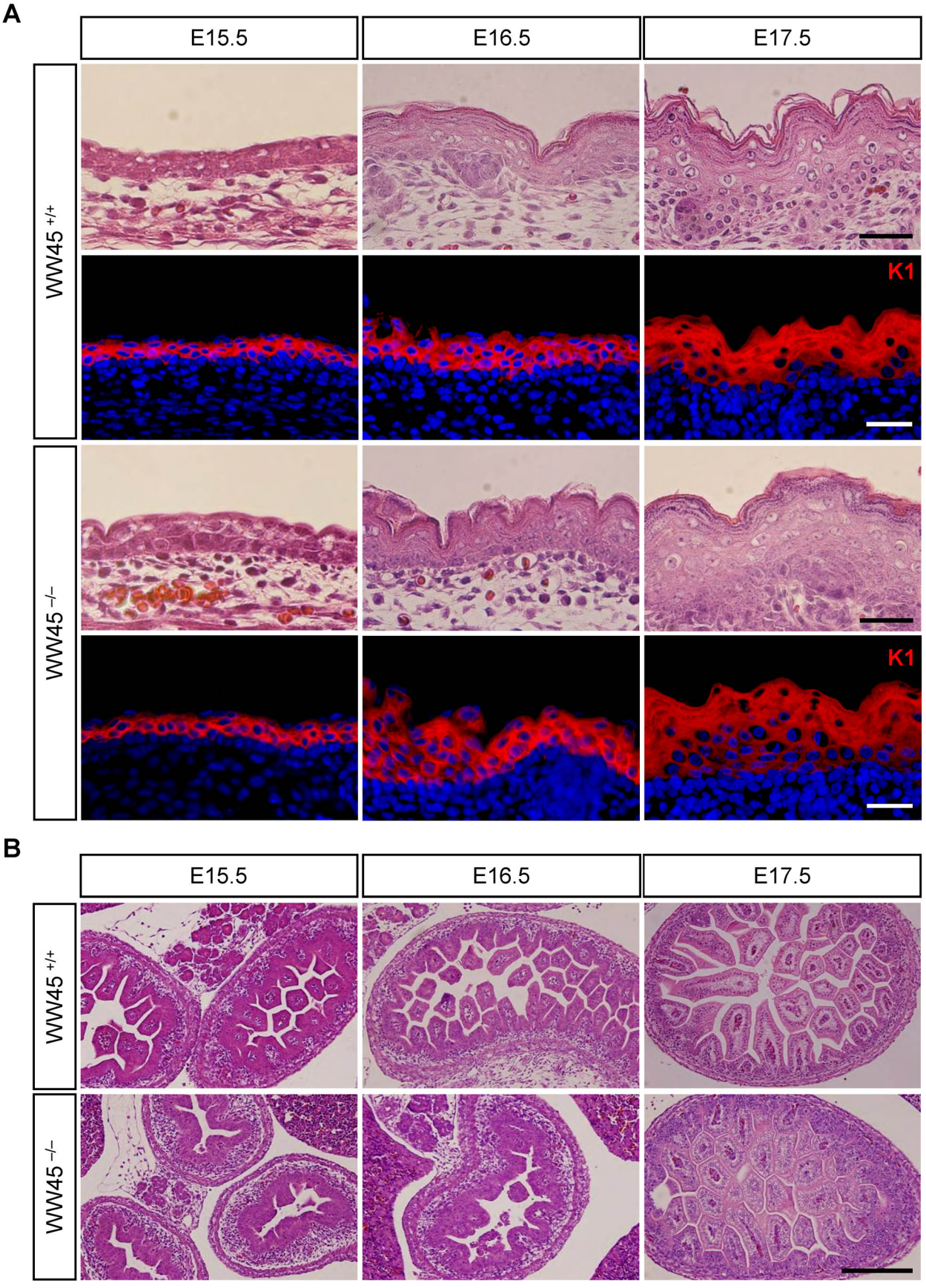

Supplemental Figure S11

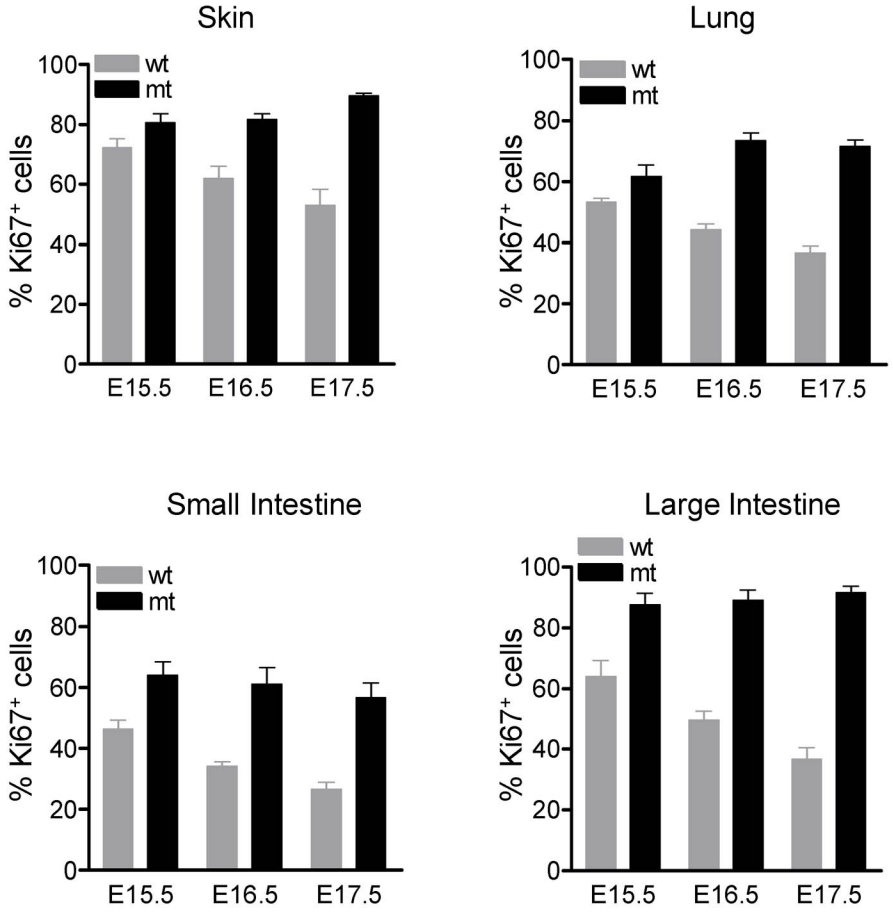

Supplemental Figure S12